

Coarse graining the dynamics of heterogeneous oscillators in networks with spectral gaps

Karthikeyan Rajendran^{1,*} and Ioannis G. Kevrekidis^{1,2,†}

¹*Department of Chemical and Biological Engineering, Princeton University, Princeton, New Jersey 08544, USA*

²*Program in Applied and Computational Mathematics (PACM), Princeton University, Princeton, New Jersey 08544, USA*

(Received 27 April 2011; revised manuscript received 7 July 2011; published 21 September 2011)

We present a computer-assisted approach to coarse graining the evolutionary dynamics of a system of *nonidentical* oscillators coupled through a (fixed) network structure. The existence of a spectral gap for the coupling network graph Laplacian suggests that the graph dynamics may quickly become low dimensional. Our first choice of coarse variables consists of the components of the oscillator states—their (complex) phase angles—along the leading eigenvectors of this Laplacian. We then use the equation-free framework, circumventing the derivation of explicit coarse-grained equations, to perform computational tasks such as coarse projective integration, coarse fixed-point, and coarse limit-cycle computations. In a second step, we explore an approach to incorporating oscillator heterogeneity in the coarse-graining process. The approach is based on the observation of fast-developing correlations between oscillator state and oscillator intrinsic properties and establishes a connection with tools developed in the context of uncertainty quantification.

DOI: [10.1103/PhysRevE.84.036708](https://doi.org/10.1103/PhysRevE.84.036708)

PACS number(s): 05.10.–a, 05.45.Xt

I. INTRODUCTION

The term *oscillator* is typically used to denote any physical system that, operating on its own (independent of neighboring oscillators), exhibits limit-cycle behavior. When such oscillators are coupled to each other, they can spontaneously synchronize. A simple, yet truly powerful model describing synchronization in oscillator assemblies is the Kuramoto model [1], which has been successfully used in many biological [2,3], chemical [4], physical [5], and social [6] contexts. This model for coupled phase oscillators and its variations have been widely studied in the literature [7]. Under specific conditions, it has been observed to exhibit complex behavior [8]. While extensive work has been performed for all-to-all coupled oscillators, real-world assemblies of oscillators are seldom globally connected to one other. Spiking neurons, for instance, are connected by a complex network structure; synchronization of such neuronal systems has been modeled using the Kuramoto model modified to account for the network topology [9]. Kuramoto oscillators with structured underlying network topologies are increasingly being investigated in the literature (e.g., Refs. [10–12]).

We consider a generic system of *nonidentical* phase oscillators connected by a network structure and explore the computer-assisted reduction of the system dynamics. Coarse graining is feasible when there is an inherent *separation of time scales* in the system, i.e., when constituent processes of the system dynamics occur at very different rates. Networks with spectral gaps (big jumps in the eigenspectrum of their graph Laplacian) can endow the coupled oscillator dynamics with this kind of time-scale separation. Our illustrative example is a simple network structure containing a spectral gap after a relatively small number of eigenvalues (sorted in ascending order) of the graph Laplacian. The small number of leading eigenvalues before the spectral gap endows the system

with *low-dimensional* long-term dynamics. The eigenvectors associated with these eigenvalues (corresponding to “slow modes”) are used to define the coarse variables useful in model reduction. Such coarse variables take into account the network structure but do not account for the fact that the oscillators in the network are *nonidentical* in terms of their angular frequencies. We will discuss how this additional heterogeneity (intrinsic to the oscillators, as opposed to the heterogeneity associated with their coupling connections in the network) can also be accounted for in the selection of a set of coarse variables (observables).

Once appropriate coarse observables are identified, one typically obtains a reduced set of equations (approximately) describing the evolution of these observables. In this paper we will circumvent this step using the so-called *equation-free* framework [13]; in this approach, short bursts of detailed system simulation are used to estimate the coarse time derivatives (actions of coarse Jacobians, etc.) required to compute solutions with the coarse variables. The use of this approach is illustrated in more detail in the Appendix.

The remainder of this paper is structured as follows: Sec. II describes our illustrative example and outlines its relevant dynamic behavior. Section III discusses possible approaches to coarse graining the system dynamics, focusing on the selection of appropriate coarse variables (observables). A first round of results of our coarse-grained computations is presented in Sec. IV; a quick review of the equation-free framework employed for these computations is relegated to the Appendix. Sections V and VI focus on the heterogeneity of the intrinsic oscillator frequencies, its effect on their states, and present an approach to account for these effects in coarse graining. Section VII concludes with a summary and discussion of possible generalizations of the approach.

II. SYSTEM DYNAMICS

Our illustrative example is a network of oscillators with a single state variable (*phase*) associated with each oscillator. These phases evolve based on the Kuramoto equations, taking

*krajendr@princeton.edu; <http://arnold.princeton.edu/~krajendr/>

†yannis@princeton.edu; <http://arnold.princeton.edu/~yannis/>

into account the particular connectivity structure:

$$\frac{d\theta_i}{dt} = \omega_i + \frac{K}{N} \sum_{j=1}^N A_{ij} \sin(\theta_j - \theta_i), \quad 1 \leq i \leq N. \quad (1)$$

Here N is the total number of oscillators in the system, θ_i and ω_i are the phases and the intrinsic angular frequencies of the individual oscillators, and K is the coupling strength, measuring the influence of every oscillator on the oscillators connected to it. The matrix A , the adjacency matrix defining the network structure connecting the oscillators, is defined as follows: $A_{ij} = 1$ if oscillators i and j communicate with each other and $A_{ij} = 0$ otherwise.

For our simulations, we use 500 oscillators with their intrinsic frequencies sampled from a Gaussian distribution with mean 0 and standard deviation $1/15$; we will discuss different distributions in Sec. VII. For the underlying connectivity we built a network with a spectral gap, which was observed to lead to low dimensionality in the long-term system dynamics; this provides the motivation for coarse graining. The target graph for our illustration was created from a collection of m subgraphs (communities) each containing s nodes; the total number of nodes (oscillators) in the final network was $N = m \times s$. Each subgraph was created using the Watts-Strogatz model [14], which contains two parameters, k —the average degree of the nodes and p —the probability of rewiring. The values of k for the m subgraphs were assigned by uniformly sampling an even number in the range between (and including) 14 and 38, corresponding to an average degree of approximately 25%–75% of the total number of nodes in the subgraph. The values of p for the individual subgraphs were sampled uniformly in a log scale between 0.001 and 1 (i.e., the values of $\log_{10} p$ are sampled uniformly between -3 and 0). The Watts-Strogatz model was chosen to create the constituent subgraphs because it creates graphs ranging from Poisson degree distribution (random) to power-law distribution (scale-free) depending on the parameter p . Once all the subgraphs (or communities) are created, a node is randomly chosen from each of the communities to be its *leader*. Now, all the m leaders are connected to each other resulting in a complete network of leaders with $\binom{m}{2}$ edges. We thus arrive at a connected graph, $\mathcal{G}^{(N,m)}$ with m communities and N nodes in total; a sample resulting graph is shown in Fig. 1 for the case of $m = 5$ and $s = 10$. In our simulations, we use a graph $\mathcal{G}^{(500,10)}$ created using the same procedure with $m = 10$ and $s = 50$. The normalized Laplacian of the graph, denoted by L , is defined as

$$L_{ij} := \begin{cases} 1 & \text{if } i = j \text{ and } d_i \neq 0, \\ -1/\sqrt{d_i d_j} & \text{if } i \neq j \text{ and } A_{ij} = 1, \\ 0 & \text{otherwise} \end{cases} \quad (2)$$

where d_i is the degree of node i .

The normalized Laplacian (in this paper, the term Laplacian should always be taken to mean the normalized graph Laplacian) corresponding to our graph $\mathcal{G}^{(500,10)}$ was computed, and its first few eigenvalues (arranged in the ascending order) are plotted in Fig. 2; there is a clear gap in the spectrum after the 10th eigenvalue.

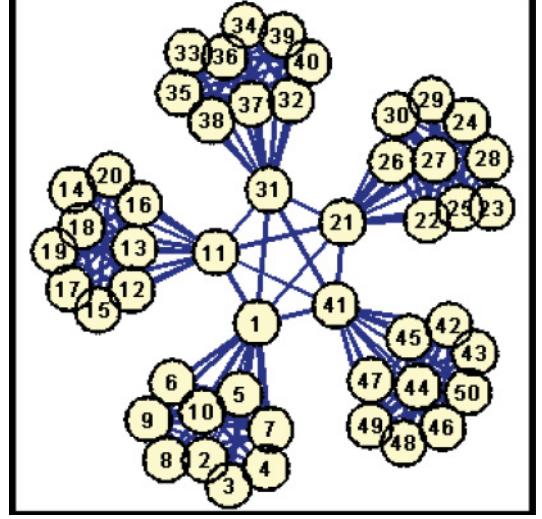


FIG. 1. (Color online) A sample graph with a spectral gap, $\mathcal{G}^{(50,5)}$, created using the procedure described in the text. (The image was created using the graph layout package for MATLAB written by Matthew Dunham, University of British Columbia.)

We perform direct simulations of the phase oscillator model (1) at different values of coupling strength, with the network topology and oscillator frequencies chosen as described above; the initial phases of the oscillators are sampled from a uniform distribution between $-\pi$ and π . All our results are reported after the instantaneous average system phase $\arg(\sum_j e^{i\theta_j})$ has been subtracted (i.e., in a frame that rotates along with the average system phase). At sufficiently large values of coupling strength K we observe (as expected) that the oscillators spontaneously synchronize their frequencies, and their phases “lock” at steady state. Representative phase evolution at such a high coupling strength $K = 0.5$ is shown at successive time steps in Fig. 3; note how the community structure of the oscillators quickly becomes visually apparent in the figure.

A quantitative measure of *phase synchronization* (or coherence in an oscillator population), the so-called *order parameter*, has been defined as

$$r = \left\| \frac{1}{N} \sum_{j=1}^N e^{i\theta_j} \right\|. \quad (3)$$

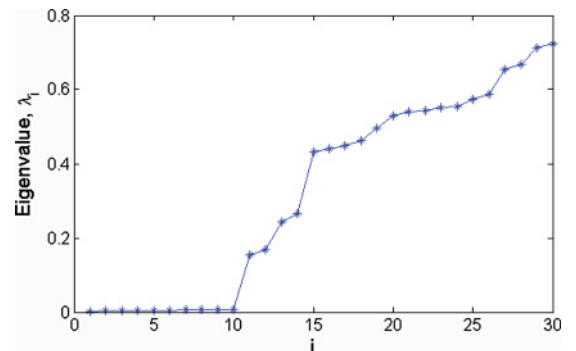


FIG. 2. (Color online) The first 100 eigenvalues of the graph Laplacian corresponding to $\mathcal{G}^{(500,10)}$.

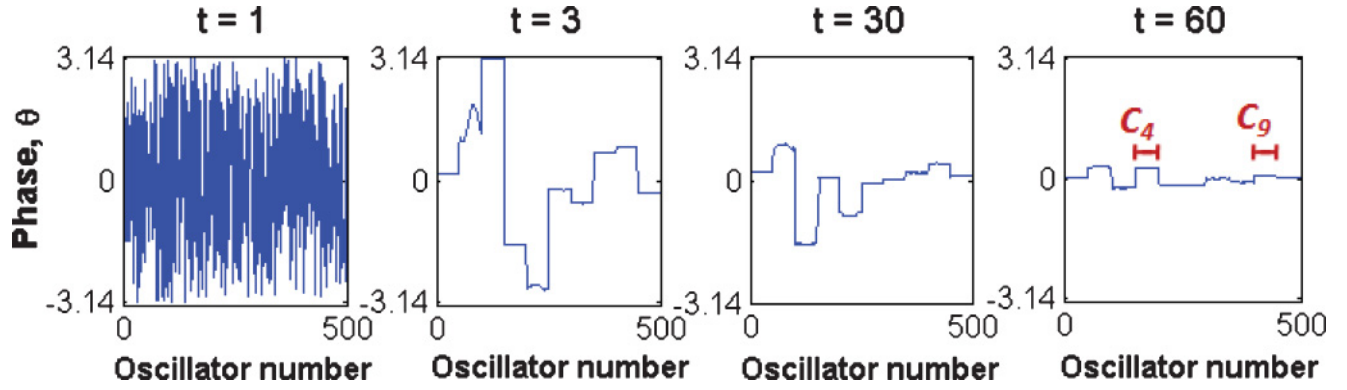


FIG. 3. (Color online) The temporal evolution of the phases of the oscillators at a coupling strength of $K = 0.5$. The oscillators in a couple of representative communities (the fourth, C_4 , and ninth, C_9) are marked in the last plot of the sequence.

Its values can range between 0 and 1. The higher the value of the order parameter, the higher the degree of synchronization: A value of 1 indicates the state where all oscillators have the exact same phase. The evolution of this order parameter is shown at a coupling strength of $K = 0.5$ as solid lines in Fig. 4. As expected (and confirmed computationally) the steady-state value of the order parameter decreases with coupling strength until a critical value of K_c ; below this critical value the oscillators do not synchronize anymore, and limit-cycle oscillations are observed initially (in parameter space), resulting from a supercritical Hopf bifurcation at K_c . The evolution of the order parameter at $K = 0.1$ depicted by the solid lines in Fig. 5 exhibits such steady limit-cycle oscillations.

III. COARSE GRAINING

Our objective is to develop and implement a computer-assisted coarse-grained model of our illustrative coupled oscillator system. The most important step in coarse graining probably consists of the selection of appropriate coarse observables: A reduced set of variables in terms of which

a useful *closed* description can be obtained. Given suitable coarse variables, it is sometimes possible to derive the reduced equations analytically (in closed form). If, however, the closures required to “write down” the reduced equations in closed form are not known, or cannot be easily approximated, the so-called equation-free framework [13,15] can be used to *computationally* implement the reduced model, circumventing its explicit derivation. A brief description of the main points of this modeling and computation framework for complex systems can be found in the Appendix.

In order to motivate our selection of coarse variables, we first identify collective features in the detailed simulation results. Consider the temporal evolution of the oscillator phases as shown in Fig. 3 (for $K = 0.5$). In our network $\mathcal{G}^{(N,m)}$, the first $s (= N/m)$ oscillators belong to the first community, the next s to the second community and so on; we define C_k as the set containing the indices of all the oscillators in the k th community:

$$C_{k \in [1,m]} = \{(k-1)s + 1, (k-1)s + 2, \dots, ks\}. \quad (4)$$

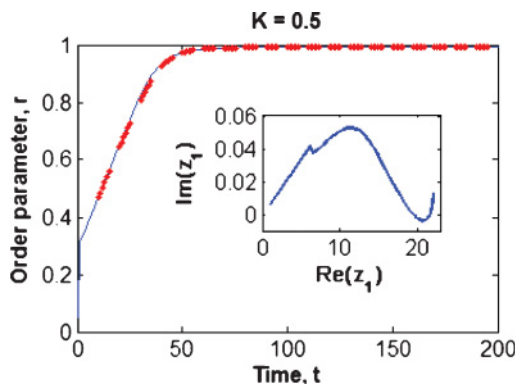


FIG. 4. (Color online) The evolution of the Kuramoto order parameter over time at a coupling strength of $K = 0.5$. The results from direct simulation are the solid lines (blue), while the results from coarse projective integration (five time steps for simulation and five for projection) are the dots (red). (The thickness of the plotted dots make the projection step appear shorter). The phase portrait in terms of the real and imaginary components of the first coarse variable [see Eq. (9)] is shown in the inset.

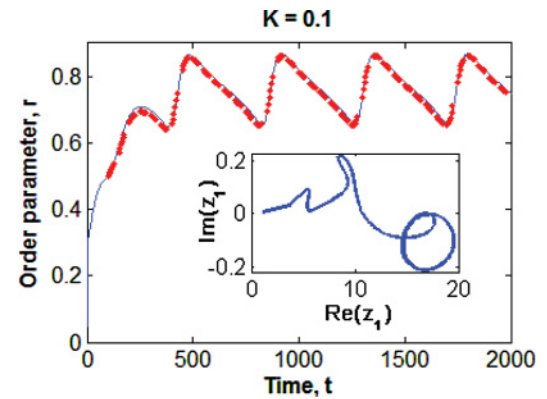


FIG. 5. (Color online) The evolution of the Kuramoto order parameter over time at a coupling strength of $K = 0.1$. The results from direct simulation are the solid lines (blue) while the results from coarse projective integration (25 time steps for simulation and 25 for projection) are the dots (red). (The thickness of the plotted dots make the projection step appear shorter). The phase portrait in terms of the real and imaginary components of the first coarse variable [see Eq. (9)] is shown in the inset.

Two oscillators within the same community are connected “more tightly” (they share more common neighbors) than oscillators in different communities. We *observe* in the simulations that the phases of all the oscillators within a community synchronize with each other at much shorter time scales than those over which the entire network synchronizes. This suggests that, because of the *construction* of our network topology, its structure can help rationalize the selection of coarse variables appropriate for the *long-term* dynamics, after initial transients quickly die out. That this separation of time scales leads to low dimensionality in the system state can be seen in Fig. 3: The randomly initialized individual oscillator phases (our “microscopic” or “fine-scale” variables, U in equation-free notation) quickly evolve to “respect” the coarse community structure of the network.

As a result, the following possibilities for coarse variables suggest themselves.

A. Option 1: Average phase in each community

An obvious choice for a set of coarse variables, $u^{(1)}$, for our example is to use a single common (time-varying) phase angle for each community. The *restriction operation* (fine states to coarse states in equation-free language) is then defined by assigning the average phase, $\bar{\theta}_k$, of all the oscillators in the k th community as the single common phase of that community [Eq. (5)]. The *lifting operation* (coarse states to consistent fine ones) is implemented by assigning this common phase as the phase angle of all the oscillators in that community (6):

$$\bar{\theta}_k = \frac{1}{s} \sum_{j \in C_k} \theta_j, \quad (5)$$

$$u^{(1)} = \{\bar{\theta}_{k \in [1, m]}\}. \quad (6)$$

This apparently intuitive coarse variable selection suffers from two drawbacks. First, partitioning the oscillators into different communities (“clustering” [16–18]) is nontrivial for a general network structure (even though, due to the particular construction, it was easy for our example). Even when community structures can be identified, however, this set of coarse variables does not take into account the differences *between* the different communities and the structure *within* the communities. This suggests an alternative set of coarse variables that uses the graph Laplacian of the network.

B. Option 2: Projection to a (truncated) Laplacian eigenbasis

Consider the normalized Laplacian matrix, defined in Eq. (2), for the graph $\mathcal{G}^{(500,10)}$. Let λ_j be the j th eigenvalue and \mathbf{v}_j the corresponding normalized eigenvector of the graph Laplacian. From Fig. 2, it can be seen that the first 10 eigenvalues are well separated from the rest (in other words, a spectral gap exists). The components of the eigenvectors of the graph Laplacian corresponding to the 10 smallest eigenvalues are plotted as connected dotted lines in Fig. 6. These eigenvectors embody, in an alternative way, the coarse community structure of the entire network. Linear combinations of these eigenvectors can be used to approximately represent any one of the individual communities [as an example, a linear combination of the first 10 eigenvectors whose support lies

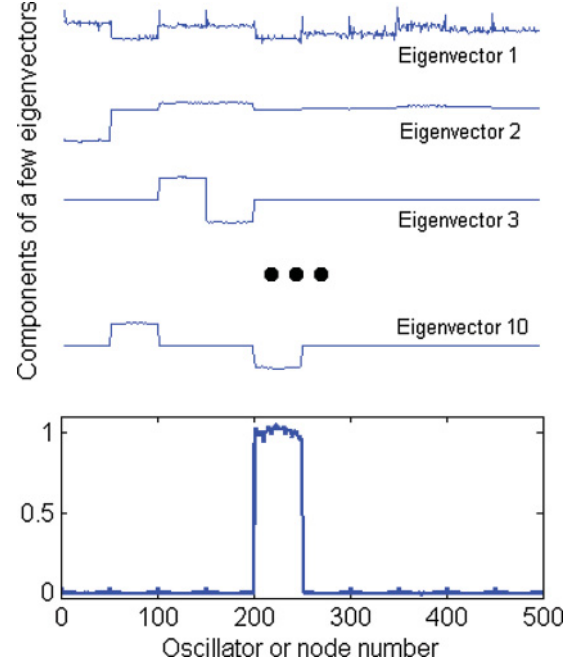


FIG. 6. (Color online) The components of a few leading eigenvectors of the Laplacian of the graph $\mathcal{G}^{(500,10)}$ are plotted in arbitrary units. The plot (blue line) at the bottom corresponds to a vector that is a linear combination of the first 10 eigenvectors; it is clearly localized to oscillators in the fifth community only. The 10 linear combination coefficients are $[2.066, 0.259, 0.004, 0.273, -0.323, 0.222, -1.151, 0.017, 4.385, -4.982]$.

(approximately) only on the oscillators in the fifth community is shown as a thick solid line in Fig. 6]. When only a few eigenvectors capture the presence and structure of the different communities, they form a suitable basis to represent the long-term dynamics of this system. A comparison of Figs. 3 and 6 also suggests that a linear combination of these eigenvectors is likely to represent well the long-term evolving states of the phase oscillators. In other words, after a short initial transient, the system becomes attracted to a *low-dimensional manifold* on which the individual oscillator phases can be represented using a lower dimensional basis formed by the first few (here 10) Laplacian eigenvectors of the network; these eigenvectors *parametrize* the low-dimensional manifold.

The use of the graph Laplacian in constructing (coarse) observables is, of course, not new [19–22]. Below we will use these variables not only as observables, but as the means to implement accelerated coarse-grained computations with the model. There is a clear analogy between such observables and the use of the finite Fourier transform in solving initial-boundary value problems: Instead of eigenfunctions of diffusion in *physical space* we have eigenvectors of the Laplacian *on a graph*; instead of evolution equations for time-dependent Fourier mode amplitudes we envision evolution equations for time-dependent components of the system phases on the first few graph Laplacian eigenvectors.

It is important to point out that the graph Laplacian also happens to be the Jacobian of the linearization of the dynamical model around the uniform solution of a “nearby” problem: that of coupled *identical* oscillators [19,20]. We consider our main working example with heterogeneous oscillators as a

(small) perturbation of the homogeneous oscillator case. If our perturbation (through oscillator heterogeneity) is small enough, the Jacobian around the steady state of our system of heterogeneous oscillators is expected to be similar—certainly in its gap structure—to the case of homogeneous oscillators. In order to quantify the relation between the dynamical Jacobian around the steady state and the graph Laplacian, we computed the steady state of our heterogeneous network at a coupling strength of $K = 0.5$. We evaluated the Jacobian of our system of ordinary differential equations around its actual steady state. We found a gap in the eigenspectrum of the Jacobian after the 10th eigenvalue, similar to the spectral gap in the graph Laplacian. We then took the first 10 eigenvectors of the linearized dynamics around the full steady state and considered relations between them and the first 10 eigenvectors of the graph Laplacian. The (10×10) inner product matrix between these two sets of different eigenvectors has the following 10 eigenvalues: 0.9993, 0.9993, 0.9993, 0.9993, 0.9995, 0.9992, 0.9992, 0.9995, 0.9995, 0.9991. Note that all the 10 eigenvalues are very close to 1. This implies that any vector in the span of the 10 eigenvectors of the dynamical Jacobian can be represented without much error using as a basis the first 10 graph Laplacian eigenvectors. This justifies our use of graph Laplacian eigenvectors to parametrize the low-dimensional slow manifold of the system of heterogeneous oscillators. As an additional step, we will also study the effect of the perturbation (the oscillator heterogeneity) on the phase evolution in Sec. V.

We start by defining an $N \times 1$ vector of *complex* phase angles of the oscillators, Θ :

$$\Theta_j = e^{i\theta_j}; j \in [1, N]. \quad (7)$$

The phase angles should be defined modulo 2π ; this complex phase vector correctly represents the phase variable on a unit circle (described by $\sin \theta$ and $\cos \theta$). We now choose as coarse variables ($u^{(2)}$) the components, z_j , of this phase vector, Θ , along the direction of the first 10 eigenvectors of the graph Laplacian:

$$L \mathbf{v}_j = \lambda_j \mathbf{v}_j; j \in [1, N], \quad (8)$$

$$u^{(2)} = \{z_{j \in [1, m]} = \mathbf{v}_j^T \Theta\}. \quad (9)$$

This projection is our *restriction*, while translation between the fine description (phases of all the N oscillators) and the coarse description is governed by Eq. (10), our *lifting* operator:

$$\sum_{j=1}^m z_j \mathbf{v}_j \rightarrow \Theta. \quad (10)$$

A third option for coarse graining, which includes additional heterogeneity considerations, is discussed in Sec. V.

IV. COMPUTATIONAL RESULTS

A. Coarse projective integration

Using the set of coarse variables $u^{(2)}$, we accelerated the network simulation using *coarse projective integration* as detailed in the Appendix. Representative results are shown in Figs. 4 and 5, reported in the form of time series of the order parameter for two values of the coupling strength, above and

TABLE I. Correlation between the detailed phases of the actual fixed point and those lifted from the converged coarse fixed-point values for each choice of coarse variables.

ρ	$K = 1$	$K = 0.5$	$K = 0.2$
Using $u^{(1)}$	0.9974	0.9975	0.9976
Using $u^{(2)}$	0.9983	0.9983	0.9983
Using $u^{(3)}$	0.9994	0.9994	0.9995

below K_c , respectively. For both these cases, the magnitude of the projective step is equal to the duration of the full simulation used to estimate the coarse time derivatives; that is, the full system (1) is simulated for only 50% of the overall evolution time. The coarse evolution in both cases clearly follows (in the “eye norm”) the resolved full direct simulation results; this demonstrates the accuracy of the equation-free approach and indirectly validates our selection of coarse variables.

B. Coarse fixed-point computation

We performed coarse fixed-point calculations (as outlined in the Appendix) using both choices of coarse variables and compared it to steady states calculated with the full model. Given an initial guess of the 10 coarse variable steady values, the coarse time stepper was constructed by lifting, followed by full model simulation (a representative time stepper horizon was $\tau = 10$) and restriction. Fixed points of the coarse time stepper were arrived at through a Newton-Krylov Generalized Minimal RESidual (GMRES) iteration [23,24].

To quantify accuracy, we calculated the pairwise linear correlation coefficient between the detailed (“fine-scale”) phases of the actual fixed point, and those lifted from the converged coarse fixed-point values for each choice of coarse variables. The results are reported in Table I for three different coupling strengths. The first (respectively, second) row corresponds to results obtained using $u^{(1)}$ (respectively, $u^{(2)}$) as coarse variables. Clearly, $u^{(2)}$ gives a more accurate coarse description

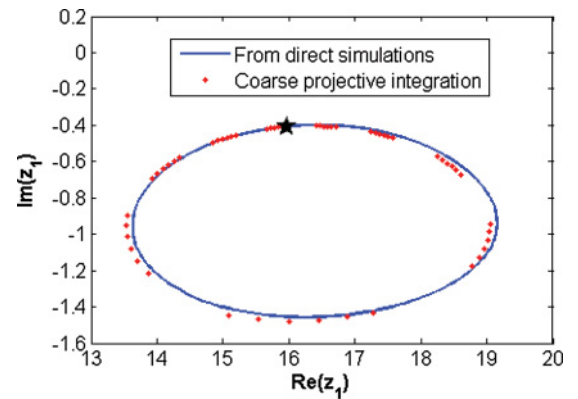


FIG. 7. (Color online) A coarse limit cycle computed from direct simulations at a coupling strength of $K = 0.1$ is plotted using a solid (blue) line. The star (black) corresponds to the solution (the point on a Poincaré map) obtained using a coarse limit-cycle solver. This point is then used as the initial condition for coarse projective integration (red dots); the coarse trajectory returns to that point after one period.

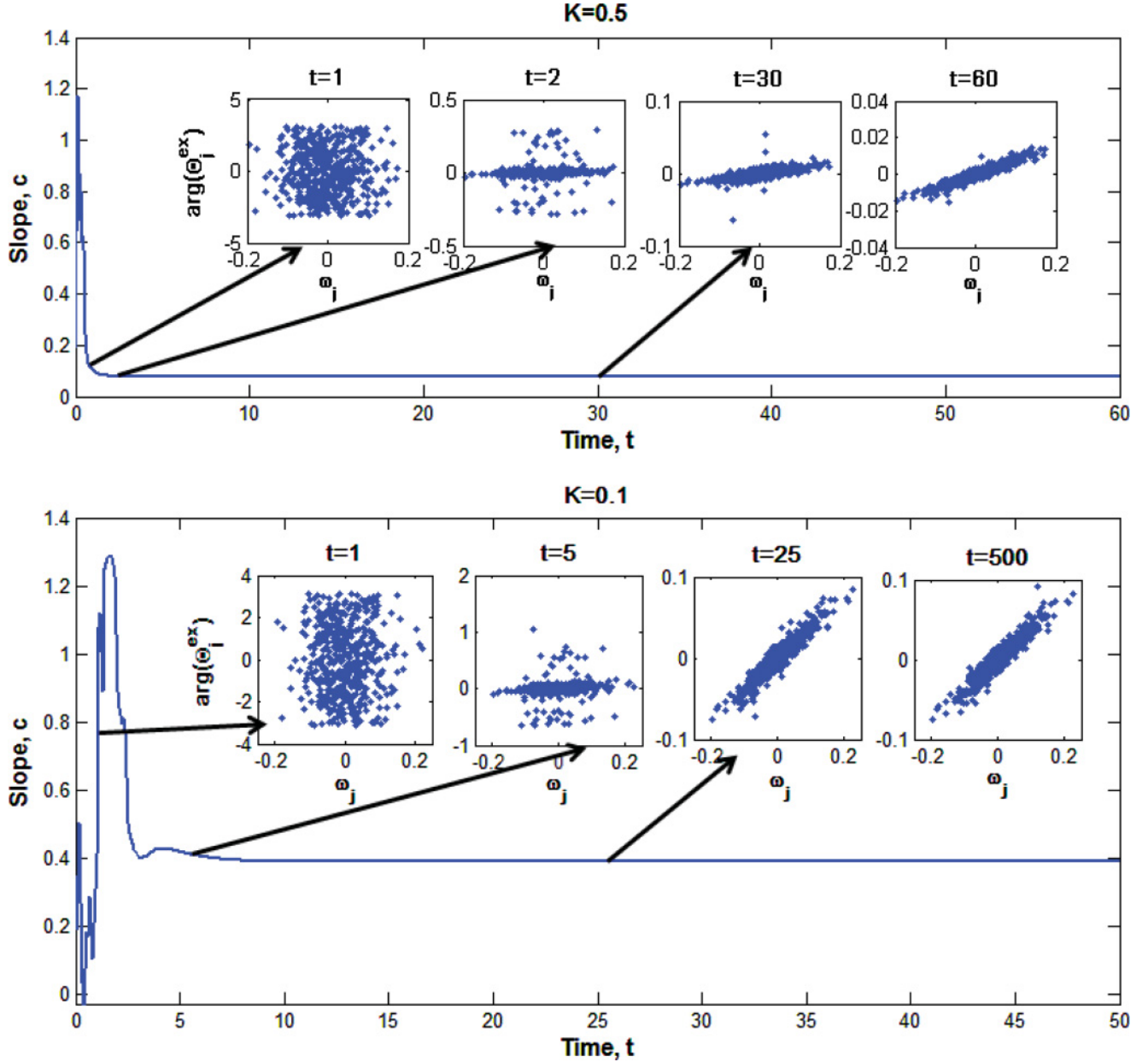


FIG. 8. (Color online) Gaussian heterogeneity distribution: Evolution of the slope c of the linear fit between excess phase and angular frequency for $K = 0.5$ and 0.1 . Insets: Plots of excess phases $\arg(\Theta_i^{\text{ex}})$ vs oscillator angular frequencies ω_j at a few representative temporal instances.

of the system fixed points compared to just using the average phases in the communities ($u^{(1)}$).

C. Coarse limit-cycle computation

We have already discussed the existence of stable limit-cycle oscillations below (and close to) the critical coupling strength K_c . The limit cycle found from direct simulations for $K = 0.1$ is plotted as a solid line in the phase-space projection on the real and imaginary parts of z_1 in Fig. 7. We also find a (coarse) point on this limit cycle by locating the (coarse) fixed point of an appropriate (coarse) Poincaré map; the point is represented as a star in Fig. 7. This point (as well as the period of the coarse limit cycle) is found by solving (again

through Newton-Krylov GMRES) Eq. (A3) for the appropriate set of values of the coarse variables $u^{(2)}$; the Poincaré map was defined in terms of the $\text{Re}(z_1)$ coarse variable. In these computations, the full system was simulated for the entire Poincaré return time; but the map and the Newton fixed-point computation were performed in the *reduced* space of the coarse variables. In an extra validation step, the trajectory around the limit cycle was followed through coarse projective integration (Fig. 7) and seen to coincide visually with the (phase space projection of the) full simulation limit cycle.

These representative computations confirm that computational coarse graining (with the appropriate selection of coarse variables) can be used to effectively perform computations with the (explicitly unavailable) coarse-grained model.

Integrating the coarse model using coarse projective integration takes about 35% less computational time than that of the full system for both the cases corresponding to Figs. 4 and 5. Computational savings also arise in coarse fixed-point and limit-cycle computations because we solve a much smaller system of equations than that required for computing the detailed fixed points and limit cycles. Coarse projective integration, coarse fixed-point, and limit-cycle computations (and also, easily, coarse stability and continuation computations) can be implemented in the form of computational “wrappers” around the full simulation. The choice of coarse variables (and the associated lifting and restriction steps) form a critical part of the approach; an improvement on this process is presented below.

V. THE EFFECT OF OSCILLATOR HETEROGENEITY

In our coarse-graining efforts, so far, we have focused on the structure of the network and ignored the effect of the heterogeneity in the angular frequencies of the oscillators. In this section we present a systematic approach to taking this heterogeneity into account in the coarse-graining procedure. The motivation comes from the observation, in the literature [25], that for all-to-all coupling (that is, in the absence of fine network structure) the oscillator phases will, under certain conditions, become *quickly* correlated with their intrinsic frequencies. We have observed the same phenomenon in our, more structured, networks: The sequence of insets in Fig. 8 shows the transient evolution of the (“excess”) phase of the oscillators in our network plotted against their individual frequencies. The term “excess phase,” Θ^{ex} , here refers to the portion of the phase vector that is not captured by the projection on the first 10 Laplacian eigenvectors; using Eq. (11) we plot the complex argument of each oscillator, *viz.*, $\arg(\Theta_j^{\text{ex}})$ against ω_j :

$$\Theta^{\text{ex}} = \Theta - \sum_{j=1}^m \mathbf{v}_j^T \Theta \mathbf{v}_j. \quad (11)$$

What we see is that, even when the oscillators are initialized with random phases (in the form of the “cloud” seen in the first inset of Fig. 8), they very quickly (visibly by time $t = 2$ and almost quantitatively by $t = 30$) develop a *strong, stationary* correlation with the intrinsic frequencies. These plots confirm the existence of a strong, approximately linear correlation between the “excess phase” and the angular frequencies of the oscillators. The evolution of the slope of the best linear fit is plotted in Fig. 8(a) and 8(b) for different values of the coupling strength K .

A number of additional observations can be made from these plots. The time taken for the correlation slope c to approach steady state is *much less* than the time scale in which the order parameters reach steady state (compare with Figs. 4 and 5). Even for the case of $K = 0.1$, corresponding to stable limit-cycle oscillations, the values of c do not vary much once the stable limit cycle is approached. Figure 9 shows how this (quickly achieved) steady-state correlation slope varies with the oscillator coupling strength. For a range of coupling strengths, this steady-state value of c is obtained for three different frequency distributions (the oscillator frequencies were sampled from the normal distribution with mean 0 and

standard deviation of 1/10, 1/15 and 1/20, respectively.) The steady-state correlation between excess phase and frequency appears to be *independent* of the range of (or the variance in) the oscillator frequencies. Figure 9 and its insets quantify the dependence of the correlation on K ; the steady-state values of c are seen to decrease with coupling strength as one might expect (since, at higher coupling strengths, the oscillator phases should exhibit less variance). In particular, an approximate inverse proportionality is computationally observed between the coupling strength K , and the steady slope c^* , quantified by the following fitted curve:

$$c^* \approx 0.0383/K. \quad (12)$$

We find it remarkable that our “decoupled” procedure, which first considers heterogeneity in the network *structure*, and only then considers heterogeneity in the *oscillator intrinsic properties* gives us so robust features for the network dynamics. Note that the constant 0.0383 applies only for the particular network used in the simulation shown. For different network structure realizations, the constant will be different.

Based on these results, we can now integrate the effects of both network structure and oscillator frequency distribution in the coarse graining of the oscillator phases (in particular, in our *lifting operator*).

VI. COARSE GRAINING THE HETEROGENEOUS OSCILLATORS

The discussions in Sec. V suggest that capturing the correlation between excess phase and intrinsic oscillator frequency can lead to a better set of coarse variables and a more accurate lifting operator for the coarse-graining process. For our illustrative example, a single additional variable, the slope c , is, as we will show, sufficient for capturing this correlation. Before we demonstrate this, however, we note the more general question: For arbitrary heterogeneity distributions (not just Gaussian as the one studied here), what is the nature and number of additional coarse variables necessary to quantitatively account for the frequency heterogeneity? We will return to this question in the last section.

Using the single scalar slope c as an additional coarse variable, we define the “corrected” vector of complex phase angles, $\tilde{\Theta}$, similar to Θ , but now taking the $c\omega_j$ into account:

$$\sum_{j=1}^m z_j \mathbf{v}_j \rightarrow \tilde{\Theta}, \quad (13)$$

$$\tilde{\Theta}_j = e^{i(\theta_j - c\omega_j)}; j \in [1, N]. \quad (14)$$

Our corrected lifting operation, going beyond the first m (here 10) eigenvectors of the graph Laplacian, is given by Eqs. (13) and (14). For the corrected restriction operation, the vector of phase angles is initially projected on the first 10 graph Laplacian eigenvectors to obtain z_j ; the “excess phases” are then used to estimate the slope c through linear regression. Our augmented set of coarse variables now reads

$$\mathbf{u}^{(3)} = \{z_{j \in [1, m]} = \mathbf{v}_j^T \tilde{\Theta}, c\}. \quad (15)$$

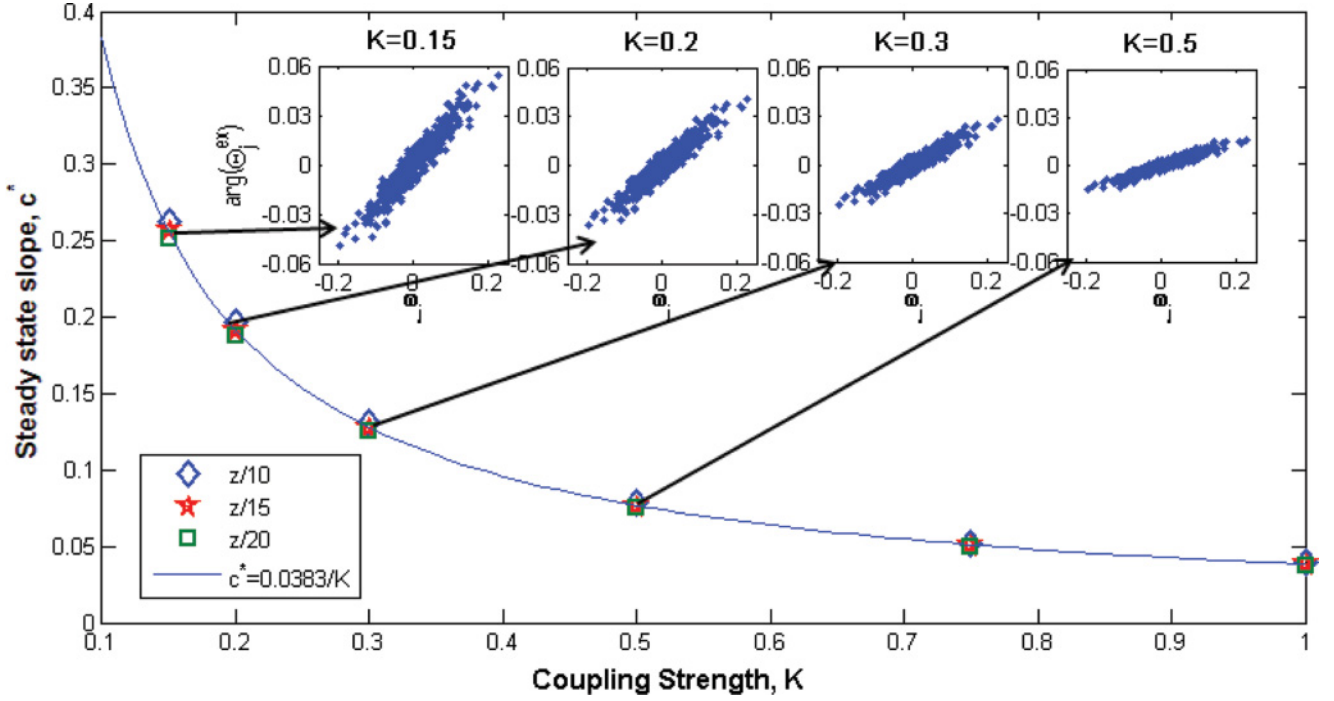


FIG. 9. (Color online) Gaussian heterogeneity distribution: Steady-state values of slope c^* of the linear correlation between excess phase and intrinsic oscillator angular frequency plotted as a function of the coupling strength K . The labels $z/10$, $z/15$, and $z/20$ in the legend denote the three different distributions from which the intrinsic oscillator frequencies are sampled, z representing a standard normal random variable. The inverse proportionality can be seen from the curve fit, $c^* = 0.0383/K$. Insets: Plots of excess phases $\arg(\Theta_j^{\text{ex}})$ vs oscillator angular frequencies ω_j at steady state for a few values of the coupling strength.

The results of computational coarse graining with the coarse variable set $u^{(3)}$ are, as one might expect, qualitatively similar to, *but more accurate than*, the results with the coarse set $u^{(2)}$ presented in Sec. IV.

Note that since (as we computationally observed) c quickly approaches an approximately constant value c^* for each specific system realization, we can, in studying long-term

dynamics, fix its value at c^* and not even consider it as an extra dynamic coarse variable. The constant value c^* for different coupling strengths can also be inferred from formulas like Eq. (12).

Each successive coarse variable choice $u^{(1)}$, $u^{(2)}$, and $u^{(3)}$ clearly includes more information about the system than the previous one: The coarse variable set $u^{(1)}$ accounts for just the presence of different communities, $u^{(2)}$ accommodates the structure of the different communities, while set $u^{(3)}$ considers the influence of the heterogeneous frequencies of the oscillators as well. In order to quantify whether this additional information is also meaningful, we compared the results of coarse fixed-point analysis using the three choices of coarse variables. The results in Table I demonstrate that the additional information included in successive choices of coarse variable sets actually leads to more accurate computation of the system features (in particular, its coarse steady states).

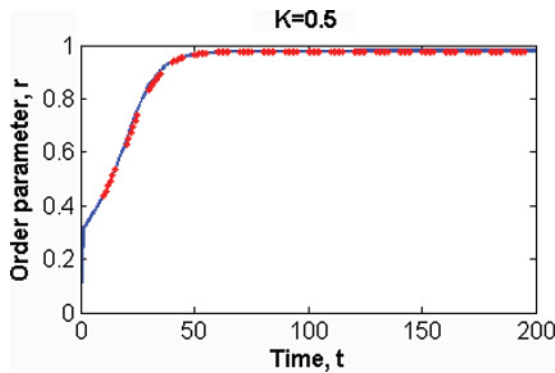


FIG. 10. (Color online) Rayleigh heterogeneity distribution: The evolution of the Kuramoto order parameter over time at a coupling strength of $K = 0.5$. The oscillator frequencies are chosen by sampling 500 numbers from a Rayleigh distribution with parameter 0.1 and then subtracting the mean from these 500 samples. The results from direct simulation are the solid lines (blue), while the results from coarse projective integration (five time steps for simulation and five for projection) are the dots (red). (The thickness of the plotted dots makes the projection step appear shorter.)

VII. CONCLUSIONS

We have demonstrated an approach to coarse graining the computations of the (long-term) dynamics of networks of coupled heterogeneous oscillators; our approach was based on the equation-free framework and was able to account, in separate steps, for the network structure and the oscillator intrinsic heterogeneity. The effect of the network structure on the evolution of the individual oscillator phases was first accounted for using the spectral properties of the network

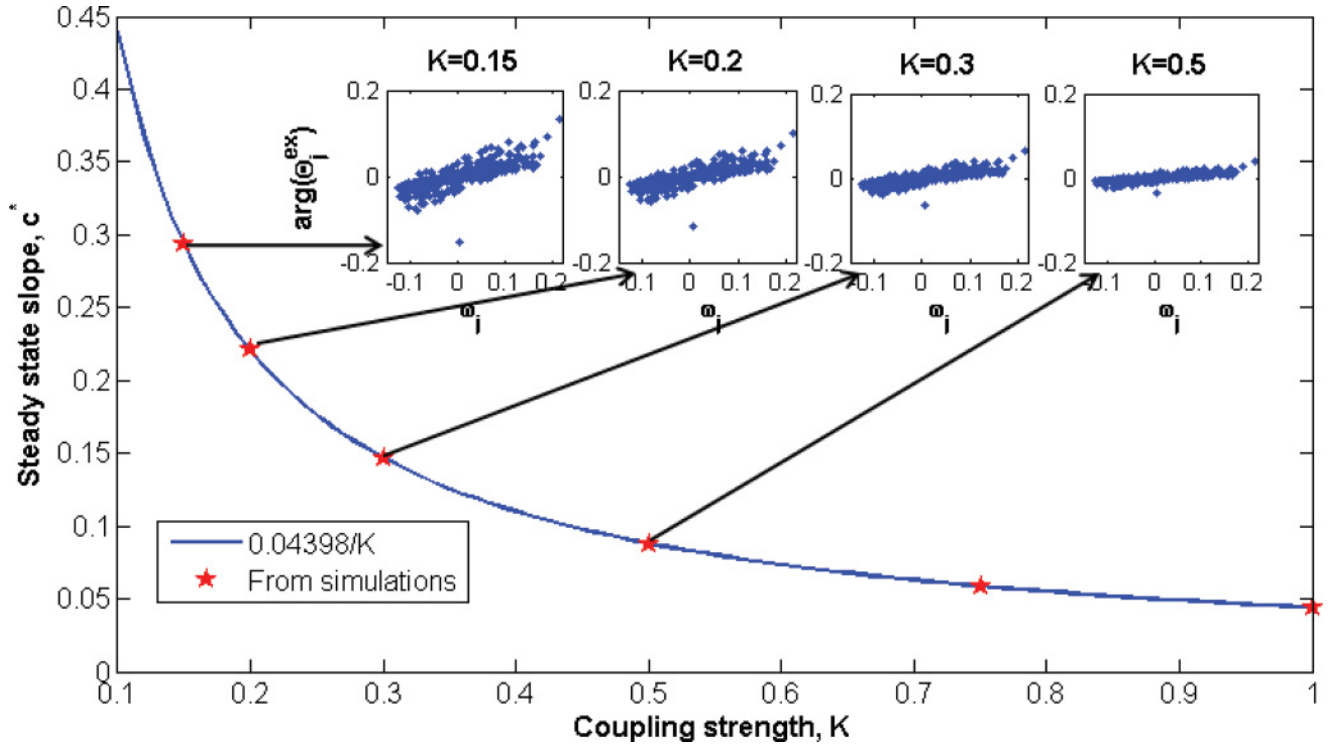


FIG. 11. (Color online) Rayleigh heterogeneity distribution: Steady-state values of slope c^* of the linear correlation between excess phase and intrinsic oscillator angular frequency plotted as a function of the coupling strength K . The oscillator frequencies are chosen by sampling 500 numbers from a Rayleigh distribution with parameter 0.1 and then subtracting the mean from these 500 samples. The inverse proportionality can be seen from the curve fit, $c^* = 0.04398/K$. Insets: Plots of excess phases $\arg(\Theta_j^{\text{ex}})$ vs oscillator angular frequencies ω_j at steady state for a few values of the coupling strength.

(under the assumption that the network graph Laplacian possesses a spectral gap). In a second step, the effect of the heterogeneity in oscillator frequencies was accounted for by observing (and then capturing) a strong correlation between (“excess”) phase angles and intrinsic oscillator frequency distribution. Both steps were incorporated in the construction of a *lifting* and a *restriction* operator (from coarse variables to detailed, fine-scale state-consistent realizations and vice versa). These operators can then be linked, in the equation-free framework, with algorithms such as coarse fixed-point and coarse limit-cycle computations, as well as with coarse projective integration, all of which were demonstrated.

We now briefly discuss the generality of our approach. As mentioned before, the graph Laplacian is close to the linearized Jacobian of our system of coupled nonidentical oscillators provided the heterogeneity in oscillator frequencies is small. This crucial observation is sufficient to guarantee a good reduction of the system using a few graph Laplacian eigenvectors as long as the system reaches the synchronized state. (This, of course, assumes that the network graph Laplacian has a spectral gap.) We study different modifications of our system in order to comment on the generality of the procedure we have outlined. First, we note that the intrinsic frequencies of the oscillators are sampled independent of the community structure in our illustrative example. This is because we study the effect of this heterogeneity as a random disturbance sampled from a known distribution. We modified our original problem and biased the

intrinsic frequencies such that oscillators in a given community have a nonzero average frequency. As a second series of modifications, we repeated the numerical experiments in our paper by sampling the intrinsic oscillator frequencies from three different distributions (uniform, exponential, Rayleigh) with mean adjusted to be 0 and variances in the same order of magnitude as in our original illustrative example. For all these modified problems, we find that we can use the graph Laplacian eigenbasis to represent the coarse evolution of the system of oscillators reaching the synchronized state.

We report representative results obtained for the specific case of oscillator frequencies sampled from a Rayleigh distribution. For this case, the intrinsic oscillator frequencies are chosen by sampling 500 numbers from a Rayleigh distribution with parameter 0.1 and then subtracting the mean from these 500 samples. The results of coarse projective integration at a coupling strength of $K = 0.5$ is shown in Fig. 10. The figure indicates that the integration of the coarse model (red dots) follows direct evolution (blue line) closely even for this case. We also study the effect of the heterogeneity in oscillator frequencies and find results that are similar to the results of Fig. 9 for the case of oscillator frequencies distributed according to a normal distribution. The excess phase becomes correlated with the oscillator frequencies as before, and the steady-state value of this correlation slope is similarly found to be inversely proportional to the coupling strength as shown in Fig. 11.

The procedure used to create the network structure used in our example, despite its apparent simplicity, creates a wide variety of networks with community structure. The Watts-Strogatz model creates graphs that can be structured or scale-free or Poisson random graphs depending on the parameter p , which we sample uniformly in a logarithmic scale from 0.001 to 1. Both the average degree and the clustering coefficients of the individual community networks vary vastly from one another. Even though the individual oscillator dynamics used for illustration here was relatively simple, we are confident that the procedures demonstrated can be extended to different, more complex individual oscillator dynamics. Extensions to networks of spiking neurons, which can also be considered as coupled oscillators—but with much more complex, and especially *directional* coupling topologies—is probably too ambitious with only these tools. As pointed out in Ref. [26], “The information required to construct a detailed and specific configuration of neocortex containing some 10^{12} connections exceeds by far the roughly 10^8 bits of information available in the genome for specification of the entire organism. On these grounds alone it appears that nature’s strategy for construction of the neocortex must depend on the dynamic assembly of rather specific but simple modules.” This reasoning supporting “module simplicity and specificity” provides hope and motivation for the deployment of reductionist approaches in such systems [27].

In our illustrative example, the (intrinsic frequency) heterogeneity distribution was simply a normal one (with different variances). A single scalar quantity (the slope, c) of the correlation between heterogeneity and system state was sufficient to improve our coarse description here. This slope is but the first nontrivial coefficient of an expansion of the system state (here, the excess phases) as a function of a random variable (here the intrinsic frequency). In effect, this is a “one-term” polynomial chaos [28] expansion of a function of a random variable (the oscillator frequency) with a particular probability distribution. It is straightforward to use different expansions (depending on the distribution of the random variable, different hierarchies of polynomials are applicable; see, for example, the Askey scheme [29]); it is also straightforward to use more than one term in the expansion in a particular polynomial set if the correlation exhibits more structure than the straight line we observed here. This research avenue provides a direct link between existing and developing tools in the study of uncertainty quantification (polynomial chaos approaches and the associated collocation schemes) with the study of coupled heterogeneous oscillator problems, even when heterogeneity arises in more than one properties of the coupled system. One particularly interesting direction for network dynamics arises when the oscillator behavior depends crucially on the *degree* of this oscillator in the overall network. If correlations between node degrees and oscillator states quickly develop in system startup transients, the tools we outlined above may well serve in successful coarse graining of the overall network dynamics.

ACKNOWLEDGMENTS

This work was partially supported by the US DOE (DE-SC0002097) and by DTRA (HDTRA1-07-1-0005).

APPENDIX: OUTLINE OF THE EQUATION-FREE FRAMEWORK

The Equation-Free (EF) approach to modeling and computation for complex or multiscale systems has been developed for problems that can, in principle, be described at multiple levels. In particular, it is applicable to systems for which the evolution equations are available at a “fine” (atomistic, microscopic, individual-based) scale, while the equations for the “coarse” (macroscopic, system level) behavior, which is of interest, are not available in closed form. We will illustrate the EF approach through a brief description of *coarse projective integration* and coarse fixed-point computation. The system of interest is completely specified at any moment in time by a set of fine or microscopic variables U . We start with the assumption that an appropriate set of coarse variables u (observables in terms of which closed equations can in principle be written at the macroscopic level) have been selected. We also assume that good *lifting* ($\mathcal{L}[\cdot]$) and *restriction* ($\mathcal{R}[\cdot]$) operators are available: The lifting creates fine-scale initial conditions consistent with prescribed values of macroscopic observables, while the restriction obtains the values of the observables from a fine-scale state. These operators effectively “translate” fine-scale states to the corresponding coarse ones, and coarse ones to consistent fine ones, respectively.

For our illustrative example, the “fine-scale” state at a time instance $t_i = i \Delta t$ is the vector of phase angles of all oscillators $U(t_i)$, while the corresponding set of coarse variable values is $u(t_i)$. A coarse projective integration step consists of the following substeps:

- (1) Lifting step: Start with initial condition $u(0)$ for the coarse macroscopic variables and lift them to a consistent microscopic description: $U(0) = \mathcal{L}[u(0)]$.
- (2) Evolve the oscillators using $U(0)$ as the initial condition for their phases in the microscopic simulator for a time t_h , long enough for the fast components of the dynamics to equilibrate, but short compared to the slow (coarse) system time scales (see Ref. [13]). The final state of this step is $U(t_h)$.
- (3) Evolve the microscopic variables, $U(0)$, for additional k time steps, generating the values $U(t_i)$, $i = h + 1$ to $h + k$, i.e., $U(t_{h+k}) = \mathcal{E}_{t_{h+k}}[U(0)]$.
- (4) Restriction step: Obtain the restrictions, $u(t_i) = \mathcal{R}[U(t_i)]$, $i = h + 1$ to $h + k$.
- (5) Projective step: Estimate time derivatives from these restrictions, $u(t_i)$, $i = h + 1$ to $h + k$, and use any numerical scheme (the simplest one would be forward Euler) to “project” the macroscopic variables “into the future” over a time interval $p \Delta t$ to obtain $u(t_{h+k+p})$.

One then uses these projected values of the coarse variables as the initial condition in repeating the overall procedure.

Using the lifting and restriction operations, and the fine-scale system simulator, one can define a *coarse time stepper* Φ_τ (A1) that takes as input the coarse variables at a given time, $u(t)$, and outputs the coarse variables at a later time, $u(t + \tau)$:

$$u(t + \tau) = \Phi_\tau[u(t)] = \mathcal{R}[\mathcal{E}_\tau[\mathcal{L}[u(t)]]]. \quad (\text{A1})$$

One can also use such a coarse time stepper to find the coarse fixed points, \hat{u} , by solving Eq. (A2) for (in principle) any time τ , using matrix-free implementations of algorithms

like Newton-Krylov-GMRES [23,24] to iteratively solve sets of nonlinear equations:

$$\hat{u} = \Phi_\tau[\hat{u}]. \quad (\text{A2})$$

With the help of coarse Poincaré maps, one can solve a similar equation to find a (coarse) point on the (coarse) limit

cycle, \tilde{u} , as well as its period, T :

$$\tilde{u} = \Phi_T[\tilde{u}]. \quad (\text{A3})$$

Matrix-free implementations of eigensolvers (e.g., matrix-free Arnoldi procedures [30]) can (and have been) used to characterize the coarse linearized stability of coarse fixed points and limit cycles [31–33].

-
- [1] Y. Kuramoto, *Chemical Oscillations, Waves, and Turbulence* (Springer, Berlin, 1984).
 - [2] F. A. O. Cruz and C. M. Cortez, *Physica A* **353**, 258 (2005).
 - [3] A. T. Winfree, *J. Theor. Biol.* **16**, 15 (1967).
 - [4] G. Ertl, *Science* **254**, 1750 (1991).
 - [5] K. Wiesenfeld, P. Colet, and S. H. Strogatz, *Phys. Rev. Lett.* **76**, 404 (1996).
 - [6] Z. Nédá, E. Ravasz, Y. Brechet, T. Vicsek, and A. L. Barabási, *Nature (London)* **403**, 849 (2000).
 - [7] J. A. Acebrón, L. L. Bonilla, C. J. Pérez Vicente, F. Ritort, and R. Spigler, *Rev. Mod. Phys.* **77**, 137 (2005).
 - [8] C. R. Laing, *Physica D* **238**, 1569 (2009).
 - [9] D. Cumin and C. Unsworth, *Physica D* **226**, 181 (2007).
 - [10] A. Arenas, A. Díaz-Guilera, J. Kurths, Y. Moreno, and C. Zhou, *Phys. Rep.* **469**, 93 (2008).
 - [11] P. Li and Z. Yi, *Physica A* **387**, 1669 (2008).
 - [12] F. Mori and T. Odagaki, *Physica D* **238**, 1180 (2009).
 - [13] I. G. Kevrekidis, C. W. Gear, J. M. Hyman, P. G. Kevrekidis, O. Runborg, and C. Theodoropoulos, *Commun. Math. Sci.* **1**, 715 (2003).
 - [14] D. J. Watts and S. H. Strogatz, *Nature (London)* **393**, 440 (1998).
 - [15] I. G. Kevrekidis, C. W. Gear, and G. Hummer, *AIChE J.* **50**, 1346 (2004).
 - [16] M. E. J. Newman, *Phys. Rev. E* **74**, 036104 (2006).
 - [17] B. Nadler, S. Lafon, R. R. Coifman, and I. G. Kevrekidis, *Appl. Comput. Harmon. Anal.* **21**, 113 (2006).
 - [18] D. Gfeller and P. De Los Rios, *Phys. Rev. Lett.* **100**, 174104 (2008).
 - [19] A. Arenas, A. Díaz-Guilera, and C. J. Pérez-Vicente, *Phys. Rev. Lett.* **96**, 114102 (2006).
 - [20] A. Arenas, A. Díaz-Guilera, and C. J. Pérez-Vicente, *Physica D* **224**, 27 (2006).
 - [21] P. N. McGraw and M. Menzinger, *Phys. Rev. E* **75**, 027104 (2007).
 - [22] P. N. McGraw and M. Menzinger, *Phys. Rev. E* **77**, 031102 (2008).
 - [23] Y. Saad and M. H. Schultz, *SIAM J. Sci. Stat. Comput.* **7**, 856 (1986).
 - [24] C. T. Kelley, *Iterative Methods for Linear and Nonlinear Equations*, Frontiers in Applied Mathematics no. 16 (SIAM, Philadelphia, 1995).
 - [25] S. J. Moon, R. Ghanem, and I. G. Kevrekidis, *Phys. Rev. Lett.* **96**, 144101 (2006).
 - [26] T. Binzegger, R. J. Douglas, and K. A. C. Martin, *Neural Netw.* **22**, 1071 (2009).
 - [27] C. Laing and G. J. Lord, *Stochastic Methods in Neuroscience* (Oxford University Press, New York, 2009).
 - [28] R. G. Ghanem and P. D. Spanos, *Stochastic Finite Elements: A Spectral Approach* (Springer, New York, 1991).
 - [29] D. Xiu and G. E. Karniadakis, *SIAM J. Sci. Comput.* **24**, 619 (2002).
 - [30] R. B. Lehoucq, D. C. Sorensen, and C. Yang, *ARPACK Users' Guide: Solution of Large-Scale Eigenvalue Problems with Implicitly Restarted Arnoldi Methods* (SIAM Publications, Philadelphia, 1998).
 - [31] G. Samaey, W. Vanroose, D. Roose, and I. G. Kevrekidis, *Comput. Methods Appl. Mech. Eng.* **197**, 3480 (2008).
 - [32] C. I. Siettos, C. C. Pantelides, and I. G. Kevrekidis, *Ind. Eng. Chem. Res.* **42**, 6795 (2003).
 - [33] K. Lust and D. Roose, *SIAM J. Sci. Comput.* **19**, 1188 (1998).